Space-resolved extreme ultraviolet (XUV) spectroscopy using a toroidal mirror

Hyun-Joon Shin, Dong-Eon Kim, and Tong-Nyong Lee
Department of Physics, Pohang University of Science and Technology, San 31 Hyoja-Dong, Pohang, Kyungbuk 790-784, Republic of Korea

(Received 9 March 1995; accepted for publication 24 March 1995)

In order to collect radiation from a distant light source and to compensate astigmatism, a toroidal mirror is often placed in front of a grazing-incidence spectrograph. In this study, characteristics of space-resolved spectra obtained with such a system have been investigated using a ray-tracing analysis. The following was found: in the stigmatic focal region of the spectrum, the spatial resolution along the sagittal direction is excellent but that along the meridional direction is poor; on the other hand, in the astigmatic wavelength region, the trend is reversed, i.e., the spatial resolution along the sagittal direction is poor but that along the meridional direction is good, particularly in the wavelength region which is far from the stigmatic focus. The method was successfully applied to the space-resolved spectroscopic study of a capillary discharge plasma. © *1995 American Institute of Physics.*

I. INTRODUCTION

A space-resolved extreme ultraviolet (XUV) spectroscopy is in great need in various scientific areas such as astronomy, soft-x-ray laser experiments, laser–plasma interaction studies, plasma fusion research, and so on. A focusing toroidal mirror has been widely used in a spectrograph equipped with a concave grating[1,2] or a variable-line-spacing grating[3] to produce a stigmatic image at a sagittal focus in various spectroscopic studies.

Even though the characteristics of a system which consists of a grazing-incidence spectrograph equipped with a spherical-grating and a toroidal mirror to correct astigmatism have been investigated in the past,[1,2,4] the spatial resolution that can be obtained with such a system is not yet well understood. One often needs to obtain space-resolved spectra from a source in a wide spectral range[5–7] and also have a space resolution both in the sagittal and meridional direction.

We have studied the spectral performance of a grazing-incidence XUV spectrograph combined with a toroidal mirror[1,2,4,8] for space-resolved spectroscopy. The method for space-resolved spectroscopy presented in this work has been applied to the spectroscopic study of capillary discharge plasmas[7] for the development of soft-x-ray lasers. In such experiments, a spatial resolution of a few hundred micrometers in the spectral range of 20–200 Å is required to selectively observe the lasing region in the capillary plasma.

II. THE OPTICAL LAYOUT

A schematic diagram of the optical layout of a concave-grating grazing-incidence spectrograph and a toroidal mirror under this study is shown in Fig. 1. Basically the toroidal mirror focuses the source in two directions with different focusing powers determined by the incidence angle and the minor and major radii of the mirror.

In the meridional plane the toroidal mirror focuses light rays from a source at the entrance slit S_1 according to the equation

$$\frac{1}{r_{st}}+\frac{1}{r_{tm}}=\frac{2}{\rho_m \cos\phi}, \tag{1}$$

where r_{st} and r_{tm} are the source-to-toroidal mirror and the toroidal mirror-to-entrance slit distance, respectively. ρ_m is the major radius of curvature of the toroidal mirror and ϕ the incidence angle to the mirror in the meridional plane.

In the sagittal plane, a stigmatic image at a given wavelength is formed at the position P' according to the combination of the grating equation and the lens equation of the spherical surface of the grating,

$$\frac{1}{r_{st}}+\frac{1}{r_{ts}}=\frac{2\cos\phi}{\rho_s}. \tag{2}$$

In Eq. (2), r_{ts} is a distance between the mirror and the image P, and ρ_s the minor radius of curvature.

The parameters of the optical system used in the present study are summarized in Table I, which are the same as those of the experimental system described later. The specific numerical values mentioned in this paper are dependent upon the parameters of an optical system; however, the basic principles drawn in this work should be true for different sets of the parameters. With these parameters the toroidal mirror forms a real image at the entrance slit with a magnification of unity ($\sim r_{tm}/r_{st}$). The acceptance angle of the system for a point source located at S is less than ± 9 mrad with respect to the optical axis in the meridional plane. The reversed real image of the source with a magnification of about 2 ($\sim r_{ts}/r_{st}$) is obtained at the sagittal focus around 287 Å. The acceptance angle in this sagittal plane is less than ± 10 mrad for a source located on the optical axis. The aberration of this system is about 30 μm at the sagittal focus in the sagittal plane.

III. EFFECT OF THE SOURCE DISPLACEMENT

In the present study, we are interested in obtaining space-resolved spectra from an elongated (8–16 mm) plasma which is produced in a capillary discharge. The spectroscopic

 0034-6748/95/66(8)/4222/5/$6.00

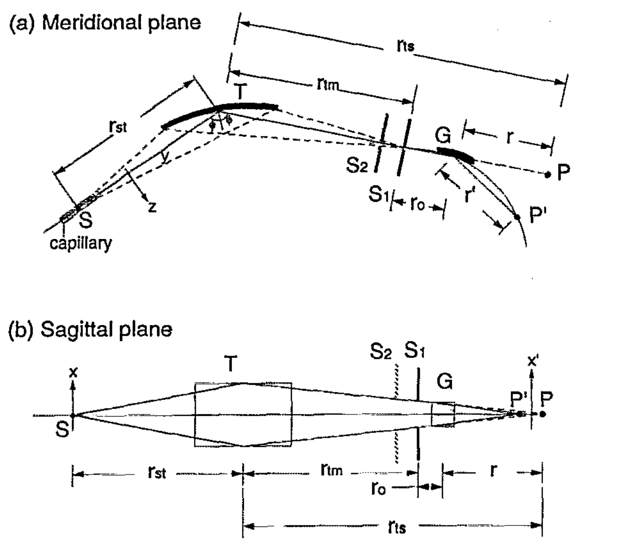

FIG. 1. Schematic diagram of the optical layout of a toroidal mirror (T) and a grazing-incidence grating (G). (a) View in the meridional plane (horizontal focus). (b) View in the sagittal plane (sagittal focus). S: point source. S_1, S_2: entrance slit and auxiliary slit. P: position of the sagittal focus. P': position of the diffracted image. ϕ: incidence angle at toroidal mirror. The y axis is defined as the optical axis.

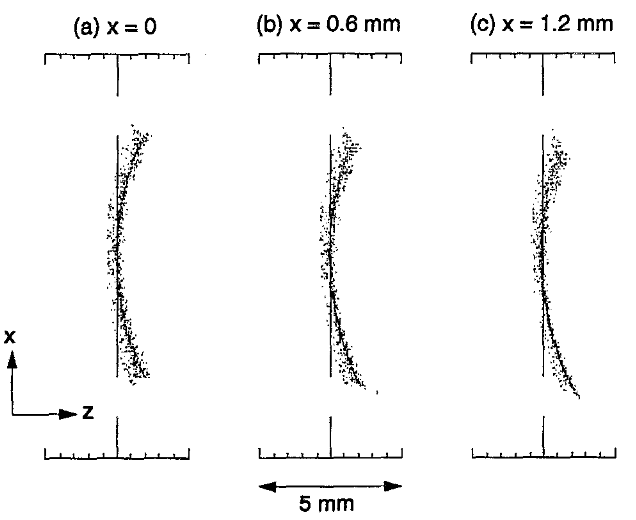

FIG. 2. The images at the entrance slit (S_1) of a source displaced along the x direction. The displacements of the source are 0, 0.6, and 1.2 mm, respectively. The slit is shown as a vertical line, the center of which the optical axis goes through. [A 10-mm-long line source (parallel to the y axis) was used in the simulation.]

observation is to be made from the end-on of the capillary with the spatial resolution in a radial direction. We assume a 10-mm-long (test) line source which is to be placed at various locations inside the capillary. The line source is always parallel to the capillary axis and to the optical axis. The optical axis is a line of sight which is determined by the toroidal mirror–spectrograph system and it is assumed to go through the center of the entrance slit. The emission from the line source diverges with an angle of ± 15 mrad meridionally and ± 20 mrad sagittally, covering the effective acceptance angle for the toroidal mirror–spectrograph system. From the ray-tracing simulation we have found that the length effect of the line source can be ignored up to 20 mm when the source is placed at the axis of the capillary. The focusing power or the image at the photographic plate for the spectral range below 200 Å varies only less than 5% for the source length variation of 4–20 mm.

When the line source is located at the optical axis, then the rays from the source form a banana-like image at the entrance slit (S_1) plane (Figs. 2 and 4). Only the rays which pass the entrance slit form diffracted images at the Rowland circle (or photographic plate), forming a stigmatic image at 287 Å for the set of parameters shown in Table I. However, when the source location is displaced from the optical axis along the x and z directions as shown in Fig. 1, the image at the entrance slit and at the film plate becomes complicated. This effect has been studied by using the ray-tracing code SHADOW.[9]

The effect of the source displacement in the sagittal plane along the x direction [the sagittal direction, Fig. 1(b)]

TABLE I. The optical parameters of the toroidal mirror–spectrograph system. r and r' are shown in Fig. 1.

Spectrograph	
Radius of curvature of the grating	R=2000 mm
Spacing between the groove lines	d=1/600 mm
Angle of incidence on grating	α'=88.5°
Sagittally focused wavelength	λ=287 Å
Angle of diffraction	β'=79.2478°
(Main) entrance slit (S_1)	22 μm×9 mm
Entrance slit (S_1)-to-grating distance	r_0=52.35 mm
Grating size (width × height)	35 mm × 25 mm
r'	373 mm
r	384.6 mm
Toroidal mirror	
Angle of incidence on mirror	ϕ=85.71°
(Major) radius of curvature of the mirror in (y,z) plane	ρ_m=605.085 cm
(Minor) radius of curvature of the mirror in (x,z) plane	ρ_s=4.538 cm
Source-to-mirror distance	r_{st}=46.3 cm
Mirror-to-entrance slit distance	r_{tm}=44.3 cm
Mirror-to-image distance	r_{ts}=88 cm
Size of the mirror	120 mm × 24 mm

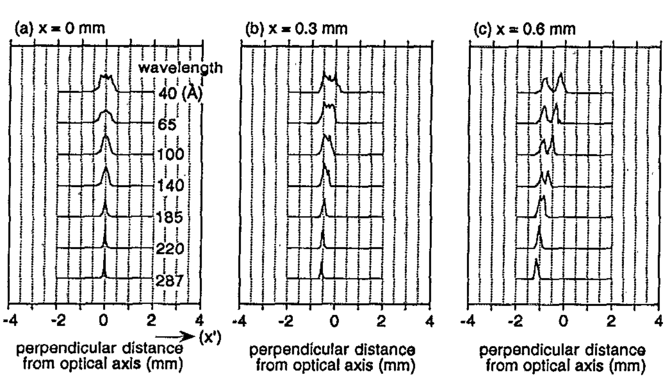

FIG. 3. The images on the Rowland circle of a source displaced along the x direction. Ray-traced intensity distributions at several wavelengths were scanned along the x' direction [Fig. 1(b)] from the optical axis. [A 10-mm-long line source (parallel to the y axis) was used in the simulation.]

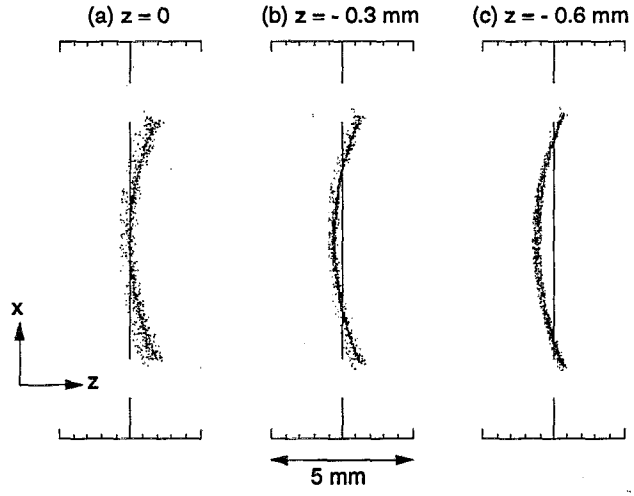

FIG. 4. The images at the entrance slit (S_1) of a source displaced along the z direction for the source locations at $z=0$, -0.3, and -0.6 mm, respectively. The slit is shown as a vertical line, the center of which the optical axis goes through. [A 10-mm-long line source (parallel to the y axis) was used in the simulation.]

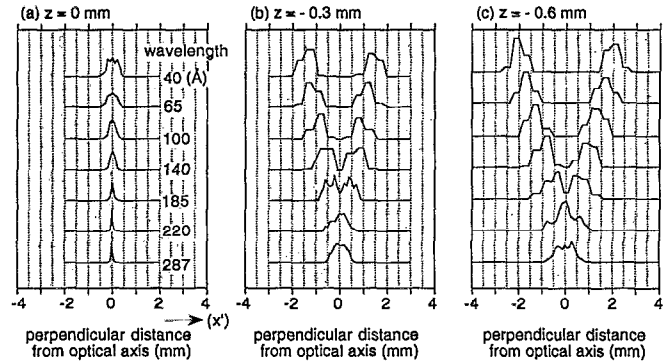

FIG. 5. The images on the Rowland circle of a source displaced along the $(-z)$ direction. Ray-traced intensity distributions at several wavelengths were scanned along the x' direction from the optical axis. [A 10-mm-long line source (parallel to the y axis) was used in the simulation.]

is shown in Figs. 2 and 3. Figure 2 shows three images of a source by a toroidal mirror at the entrance slit when the source is displaced by 0, 0.6, and 1.2 mm along the x direction [Fig. 1(b)], respectively. No appreciable change is noticed in the shape when the source displacement is less than ± 0.6 mm and the throughput (the number of rays passing through the slit) is not decreased appreciably ($<20\%$) until the source is moved by ± 2 mm.

Figure 3 shows the intensity distribution along the direction perpendicular to the dispersion on the Rowland circle for several wavelengths, when the source is located at $x=0$, 0.3, and 0.6 mm, respectively. As can be seen in Fig. 3(a), the stigmatic image is formed at 287 Å and the FWHM (full width at half maximum) of the intensity distribution is less than 35 μm. At this stigmatic wavelength the position of an image is sensitive to the position of a source in the x direction. As a source moves away from the optical axis, the spatial aberration increases the width of the intensity distribution. The FWHMs of the intensity distribution are 45 and 150 μm for $x=0.3$ and 0.6 mm, respectively. Therefore we can get a spatial resolution less than 150 μm at this stigmatic wavelength along the x direction for the source displacement less than ± 0.6 mm. On the other hand, at astigmatic wavelengths their image positions are less sensitive to the source displacements in the x direction and their widths are rather broad. For these wavelengths the spatial resolutions are worse and, as well, considerably depend on the scanning window size of a microdensitometer. For example, a 40 Å wavelength, the spatial resolution at the optical axis is ~ 800 μm when a film is read with a 300 μm wide microdensitometer window.

When the source is displaced along the z direction [Fig. 1(a)], the image formed at the entrance slit would look like Fig. 4. The source is displaced by 0, 0.3, and 0.6 mm along the $(-z)$ direction, respectively. The location of the image relative to the slit changes rather sensitively to the source displacement. When the source is displaced along the $(+z)$ direction, the number of rays passing through the slit decreases rapidly and nothing could pass through even when the source is moved only by about $+50$ μm. A number of rays passing falls down below one half when the source moves by 30 μm along the $(+z)$ direction. This tolerance of 30 μm is partly due to the length of the source and when the point source is used, this tolerance gets even smaller.

When the source is displaced along the $(-z)$ direction, two portions of its image cross with the slit and the rays which pass through the slit result in two narrow bands at the dispersion plane which converge gradually toward the focus at the stigmatic wavelength. A microdensitometer scan of the resulting spectral plate along a direction perpendicular to the dispersion would give two peaks, in general, as can be seen in Fig. 5. The separation of these two peaks increases as the wavelength decreases. At a given wavelength, particularly at shorter wavelength region, however, it is sensitively dependent on the source displacement along the $(-z)$ direction. For example, using a scan window of 300 μm, one can get a spatial resolution of ~ 50 μm at 40 Å and 100 μm at below 200 Å, respectively. At the stigmatic wavelength, however, this spatial resolution along the z direction is poor.

An extended source in the place of a line source is considered based on the above result. Suppose uniformly distributed rays coming out of a x-z plane. The resulting spectrum from such an extended source will show the spectral lines and continua with their height minimum at the stigmatic wavelength and gradually become high toward the short-wavelength region. The spatially resolved spectrum may be obtained by scanning the resulting spectral plate along the dispersion at the middle of the spectral height, for example. The spatial resolution obtainable is therefore dependent on the wavelength and the microdensitometer scan window size. Now suppose we put the scanning window at the center of the spectral height at the dispersion plane and examine a number of rays which would pass through the window at three different wavelengths. Figure 6 shows the result obtained using the ray-tracing code where the cell size was 50 μm$\times$50 μm. The origin of each plot indicates the optical axis and only a part of $x \geqslant 0$ is plotted due to the symmetry about the x axis. From these plots, one can get an idea as to

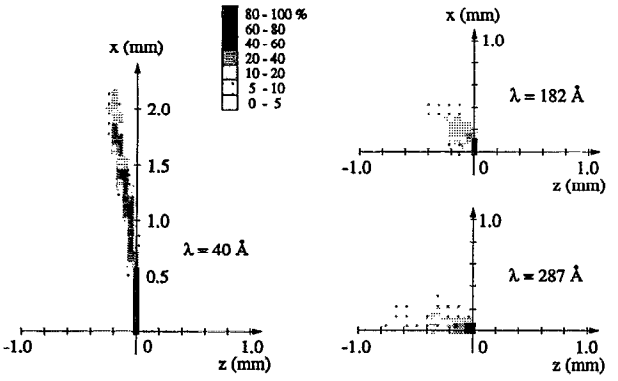

FIG. 6. Spatial resolution at the source plane (x-z plane) for wavelengths of 40, 182, and 287 Å obtained with a 300 μm microdensitometer scan window. The relative number of rays starting from each sampling point in the source plane and passing through the microdensitometer scan window is plotted. The origin for each figure is the location of the optical axis. Only the parts of $x \geqslant 0$ are plotted due to the symmetry along the x direction. The sampling size is 50 μm×50 μm. [A 10-mm-long line source (parallel to the y axis) was used in the simulation.]

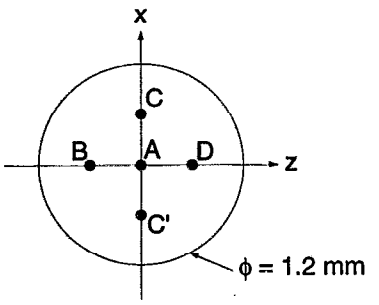

FIG. 7. Optical axis positions to observe peripheral plasma in a ϕ=1.2 mm diameter capillary discharge.

what portion out of the extended source the toroidal mirror–spectrograph system actually sees at three different wavelengths. At the stigmatic wavelength (287 Å) region, one can get good spatial resolution in the x direction but poor in the z direction. However, the trend is reversed at the 40 Å region where spatial resolution along the x direction is not good but is very good in the z direction. At an intermediate-wavelength region the spatial resolution is somewhere between the two. At the 182 Å region, the spatial resolution is about 180 μm along the -z direction and is 400 μm along the x direction. Note that for all wavelengths the spatial resolution along the $(+z)$ direction is excellent and is less than 30 μm. The overall spatial resolution can be improved by choosing the proper stigmatic wavelength according to the needs and also the narrower scanning window size.

IV. SPACE-RESOLVED SPECTRA FROM A CAPILLARY DISCHARGE

The above technique is applied to an end-on observation of a capillary discharge plasma.[7] In this experiment, we are interested in obtaining spectrum from a peripheral plasma region without seeing the plasma radiation from the central region and vice versa. It is expected that a soft-x-ray amplification takes place along the peripheral plasma region due to a rapid recombination of fully stripped carbon plasma. Polyethylene capillaries with a bore diameter of 1.2 mm were used and the covered spectral range was 20–200 Å.

Figure 7 shows the candidate locations of the optical axis (A, B, C, C', D) in the capillary cross section, in order to observe the peripheral region of the capillary without seeing the plasma radiation from central (or axial) portions. The points B, C, C', and D are located 300 μm away from the capillary axis. The features of each position are as follows:

(a) The optical axis at the point A: At the sagittal focus (at 287 Å) the spatial resolution is good (~35 μm) along the x axis as shown in Fig. 6, and one can observe the cold plasma located at 0.3 mm away from the capillary axis by reading the film 0.6 mm off the center of the spectral height in the dispersion plane (the magnification is ~2). However, for wavelengths below 200 Å it is difficult to obtain and read a portion of the spectral image of the cold plasma. The radiation background from the hot plasma could give errors in reading the portion from the cold plasma.

(b) The optical axis at C or C': At this location the system sees the cold region directly near the sagittal focus. However, at shorter wavelengths, e.g., at wavelength of 40 Å, the portion from the hot central plasma also contributes to the spectral image, as can be seen in the Fig. 6, and worsens the spatial resolution.

(c) The optical axis at B: This location might be the best of all if one wants to eliminate the contribution from the axial plasma. In this case the spectral image in the whole dispersion plane is formed only by the light from the peripheral region, $z<-0.27$ mm.

(d) The optical axis at D: This is also a good location. At the sagittal focus the spatial resolution is bad, but insofar as two peaks appear at the desired wavelength range, one can get a spatial resolution. For example, in the wavelength region below 200 Å, one can get the spectrum exclusively for the peripheral plasma which is located at $z=0.3$ mm. This location is also useful to check the alignment by measuring the distance between the two peaks; this is because the distance between the two peaks is sensitively dependent on the source displacement along the $(-z)$ direction.

Using the technique described above, we have been able to obtain spectra from the axial and the peripheral plasma regions of the capillary discharge, respectively, adopting the locations A and B as the optical axis. Figure 8(a) and 8(b), respectively, shows the resulting spectra from the axial and the peripheral region, obtained with the same optical parameters described above and also under the same discharge condition. One can see the large difference in the spectral feature between the two. The axial plasma is believed to be hotter than the peripheral region. This is manifested by the fact that the higher n members of Lyman series are strong and the temperature estimated by the slope of C VI recombination continua is higher (25 eV) in the axial plasma than that obtained (13 eV) from the peripheral plasma.[7]

V. DISCUSSION

Space-resolved spectral data obtained using a toroidal mirror grazing-incidence spectrograph system have been in

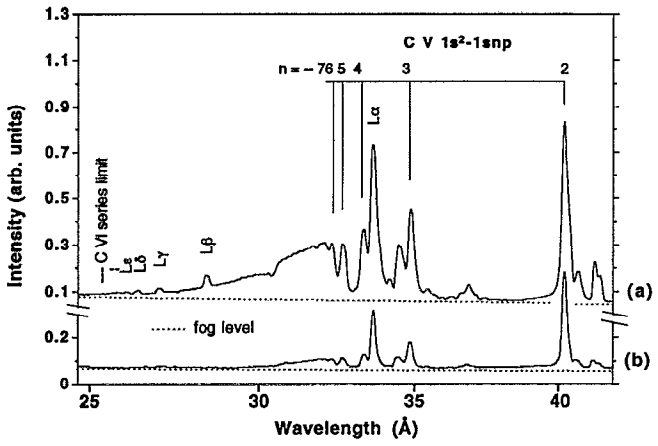

FIG. 8. Space-resolved and time-integrated spectra of (a) hot plasma and (b) cold plasma in the capillary discharge (14 mm long and 1.2 mm diameter). The discharge parameters and other conditions are the same for both cases, except for the relative location of the optical axis. The optical axis for (a) and (b) is placed at A, B of Fig. 7, respectively. (a) and (b) were obtained by scanning the spectra along the midpoint of spectral height. The measured temperatures are 25 eV for (a) and 13 eV for (b), respectively.

vestigated. The sagittal and meridional resolution of a light source at stigmatic as well as astigmatic wavelength regions have been analyzed using the ray-tracing calculation for different positions of a 10-mm-long test line source. The spatial resolutions in the both directions are determined from the relative location of optical components, the width of the entrance slit, and the scan window size of the microdensitometer. It has been shown that a good space resolution in a sagittal and a meridional direction is obtained, respectively, at the stigmatic and the astigmatic wavelength region. Particularly, an excellent space resolution in a meridional direction can be achieved in the spectral region which is far (say, 40 Å) from the stigmatic wavelength. At the intermediate-wavelength region, however, the spatial resolutions in this direction are between the two.

It has been shown for the present optical parameters where the stigmatic wavelength is at 287 Å that the spatial resolution in the meridional direction is less than 200 μm in the 20–200 Å range, when the spectrum is read by a 300 μm microdensitometer window. Another feature of the system is that the spatial resolution along the $(+z)$ direction is less than 30 μm for all wavelengths. The spatial resolution can be improved considerably by carefully choosing the optical parameters and stigmatic wavelength according to the needs.

The method suggested in this work has been applied successfully to an end-on observation of plasma which is generated in an 1.2-mm-diameter capillary discharge. In this experiment, emission spectra from the axial as well as from the peripheral plasma regions of the capillary discharge have been obtained, in order to prove the x-ray amplification in the latter plasma region.

ACKNOWLEDGMENTS

The authors would like to thank J. S. Koog for his earlier help in this work. This research was partly supported by the 1994 basic research grant from Research Institute of Science and Technology, the Korea Science and Engineering Foundation, and the Basic Science Research Program of the Korean Ministry of Education.

[1] G. Tondello, Opt. Acta **26**, 357 (1979).
[2] E. Jannitti, P. Nicolosi, and G. Tondello, Opt. Lett. **4**, 187 (1979).
[3] P.-Z. Fan, Z.-Q. Zhang, J.-Z. Zhou, R.-S. Jin, Z.-Z. Xu, and X. Guo, Appl. Opt. **31**, 6720 (1992).
[4] J. A. R. Samson, *Techniques of Vacuum Ultraviolet Spectroscopy* (Wiley, New York, 1967).
[5] R. A. McCorkle and H. J. Vollmer, Rev. Sci. Instrum. **48**, 1055 (1977); R. A. McCorkle, Appl. Phys. A **26**, 261 (1981).
[6] J. J. Rocca, O. D. Cortazar, B. Szapiro, K. Floyd, and F. G. Tomasel, Phys. Rev. E **47**, 1299 (1993); J. J. Rocca, J. C. Marconi, and F. G. Tomasel, IEEE J. Quantum Electron. **29**, 182 (1993).
[7] Hyun-Joon Shin, Dong-Eon Kim, and Tong-Nyong Lee, Phys. Rev. E **50**, 1376 (1994).
[8] W. A. Rense and T. Violett, J. Opt. Soc. Am. **49**, 139 (1959).
[9] B. Lai, K. Chapman, and F. Cerrina, Nucl. Instrum. Methods A **266**, 544 (1988); B. Lai and F. Cerrina, Nucl. Instrum. Methods A **246**, 337 (1986).